Available online at www.sciencedirect.com
ScienceDirect
Trans. Nonferrous Met. Soc. China 26(2016) 3135−3146
Transactions of Nonferrous Metals Society of China
www.tnmsc.cn

Microstructure and mechanical properties of laser beam welded TC4/TA15 dissimilar joints

Wei-feng XU[1,2], Zhen-lin ZHANG[1,2]

1. State Key Laboratory of Solidification Processing, Northwestern Polytechnical University, Xi'an 710072, China;
2. Shaanxi Key Laboratory of Friction Welding Technologies,
Northwestern Polytechnical University, Xi'an 710072, China

Received 25 December 2015; accepted 5 July 2016

Abstract: The microstructure and mechanical properties of laser beam welded dissimilar joints in TC4 and TA15 titanium alloys were investigated. The results showed that the coarse columnar grains containing a large amount of acicular α and martensite α' were present in the fusion zone (FZ), some residual α phases and martensite structure were formed in the heat-affected zone (HAZ) on TC4 side, and bulk equiaxed α phase of the HAZ was on TA15 side. An asymmetrical microhardness profile across the dissimilar joint was observed with the highest microhardness in the FZ and the lowest microhardness in TA15 BM. The orders of yield strength and ultimate tensile strength were as follows: TC4 BM > TC4/TC4 similar joint > TA15 BM > TA15/TA15 similar joint > TC4/TA15 dissimilar joint, and increased while hardening capacity and strain hardening exponent decreased with increasing strain rate from 1×10^{-4} s^{-1} to 1×10^{-2} s^{-1}. The TC4/TA15 dissimilar joints failed in the TA15 BM, and had characteristics of ductile fracture at different strain rates.

Key words: laser beam welding; titanium alloy; dissimilar joint; strain rate; microstructure; mechanical properties

1 Introduction

Titanium alloys have been widely used as structural materials, especially in the fields of aeronautics and astronautics, due to their low specific gravity, high specific strength, excellent fatigue and corrosion resistance and superior mechanical properties at high temperatures [1−4]. TA15 alloy, namely Ti−6Al−2Zr−1Mo−1V, which is a kind of near alpha titanium alloys, has been widely used as structural components of aircraft [5]. TC4 alloy (Ti−6Al−4V), as one of typical alpha-beta titanium alloys, is regarded as a structure titanium alloy with best application prospects, and more than 50% titanium alloy is TC4 alloy. To maximize its light-weighting role, the manufacturing of "hybrid" components from a variety of titanium alloys via proper welding is necessary [6].

There are several welding technologies which can be used to join titanium alloys such as tungsten inert-gas welding, metal inert-gas welding, electron beam welding and laser beam welding (LBW). LBW has drawn particular attention on titanium welding because of its high energy density, low residual stress and high productivity. Compared with electron beam welding, LBW does not need a vacuum environment, and it is more convenient, facile and saving. Besides, it is easy for titanium to get larger depth-to-width ratio of LBWed joint due to some special physical characteristics like lower thermal conductivity and higher infrared light absorptivity [7].

The microstructure, microhardness distribution and mechanical properties of the LBWed joints of dissimilar titanium have been investigated [8−10]. For example, LEI et al [8] found that HAZ of TC4 side of LBWed Ti−22Al−27Nb/TC4 joint mainly consists of a mixture of martensite α', acicular α, and primary α phase, and the ultimate tensile strength of the joints can reach about 92% that of TC4 BM, while the elongation is less than 40% that of TC4 BM. QIAN et al [9] studied the microstructure of TA2/TA15 graded structural material and reported that microhardness distribution of the joint

Foundation item: Project (51405392) supported by the National Natural Science Foundation of China; Project (20136102120022) supported by the Research Fund for the Doctoral Program of Higher Education of China; Project (3102015ZY023) supported by the Fundamental Research Funds for the Central Universities, China

Corresponding author: Wei-feng XU; Tel: +86-29-88492624; Fax: +86-29-88492624; E-mail: xwf1982@.nwpu.edu.cn

DOI: 10.1016/S1003-6326(16)64445-X

was asymmetric, which was the result of the solid solution strengthening and the grain boundary strengthening. Besides, the mechanical properties of LBWed BTi−643S/TA15 dissimilar joint were also tested at 550 °C and found that the tensile strength drastically declined, but the tensile ductility was greater than that obtained at room temperature [10]. And some other scholars explored the possibility of laser beam welding of other different materials like titanium and aluminum [11,12], titanium and stainless steel [13]. However, there are almost no related reports about the effect of strain rate on dissimilar titanium joint and it is unclear what microstructure characteristics would be present and how mechanical properties at different strain rates would change in LBWed dissimilar TC4 and TA15 titanium alloys. The objective of this study is, therefore, to examine the microstructure evolution and explore effects of strain rates on tensile properties of LBWed TC4/TA15 joints at different welding speeds and laser powers.

2 Experimental

Two kinds of annealing rolled plates of titanium alloys were utilized for laser beam welding with dimensions of 200 mm × 80 mm × 2.5 mm. The microstructure of TC4 titanium alloy is composed of α phase and fine β phase which is distributed at the elongated α grain boundaries, as shown in Fig. 1(a). The microstructure of TA15 titanium alloy consists of primary α phase and a small amount of β phase, as shown in Fig. 1(b). And the chemical composition of titanium alloys is listed in Table 1. LBW was performed using YLS−4000 fiber laser which has a focal length of 250 mm and a diameter of focused light spot of 0.33 mm. Based on prior researches, these experiments which adopted different welding speeds and laser powers were used to explore the effect of welding parameters on welded joints. In order to protect the welded joint from oxidation, high purity argon was employed as a front shielding gas, a positive shielding gas and a back shielding gas with flow rates of 15, 25 and 10 L/min, respectively (Fig. 2). Table 2 shows the welding parameters (welding speeds and laser powers) of LBWed TC4 and TA15 titanium alloy joints.

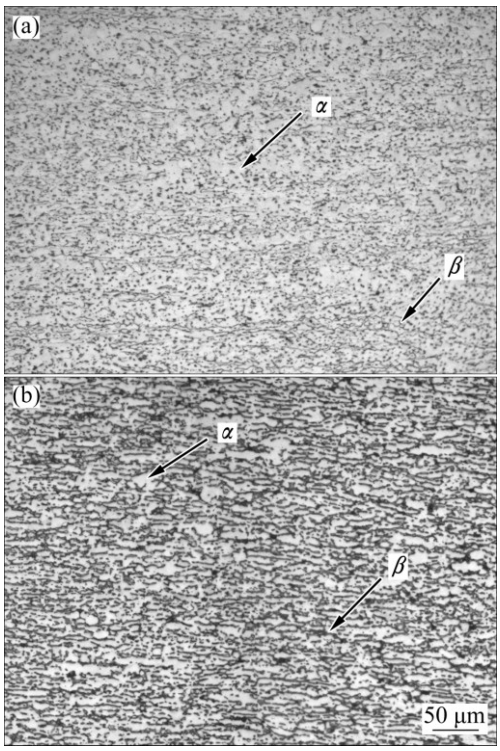

Fig. 1 Microstructures of base materials: (a) TC4 titanium alloy; (b) TA15 titanium alloy

Table 1 Chemical composition of titanium alloys

Material	Mass fraction/%					
	Al	V	Fe	C	Mo	
TC4	6.06	3.92	0.30	0.013	−	
TA15	6.72	2.32	0.08	0.0053	1.77	
Material	Zr	Si	N	H	O	Ti
TC4	−	−	0.014	0.0014	0.15	Bal.
TA15	2.19	0.14	−	−	−	Bal.

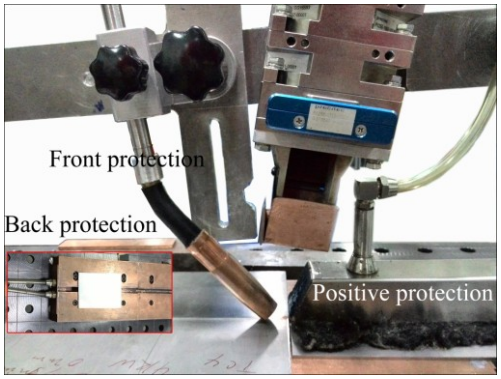

Fig. 2 Gas protective device of laser welding

Table 2 Welding parameters of titanium alloys

Test No.	Laser power/kW	Welding speed/ (m·min^{-1})	Type of joint
1	4.1	5	Dissimilar joints
2	4.1	4	Dissimilar joints
3	4.1	3	Dissimilar joints
4	4.1	2	Dissimilar joints
5	3.3	2	Dissimilar joints
6	2.5	2	Dissimilar joints
7	4.1	4	Similar joints of TC4
8	4.1	4	Similar joints of TA15

Metallographic samples were cut from LBWed joints perpendicular to the welding direction, then

ground, polished and etched using a kind of reagent (V(HF):V(HNO_3):V(H_2O)=13:7:80). Microstructures were examined via optical microscopy (OM). Vickers microhardness test was performed on the cross-section of LBWed joints perpendicular to the welding direction using a computerized HX−1000 microhardness tester at a load of 500 g and a duration of 15 s. The distances between any two consecutive indentations in thickness and in width were set as 0.3 and 0.2 mm, respectively. The 2.5 mm-thick tensile specimens with a gauge length of 25 mm and a width of 6 mm in accordance with ASTM E8 standard were machined perpendicularly to the welding direction using electro-discharge wire cutting (Fig. 3). The gauge area was hand-ground progressively along the loading direction with 120, 240, 320 and 600 grit SiC paper to remove the cutting marks and to achieve a smooth surface. Tensile testing was performed using an INSTRON−3382 testing machine under different strain rates (1×10^{-2}, 1×10^{-3} and 1×10^{-4} s^{-1}) at room temperature. The fracture surfaces of BM and LBWed joints were observed using scanning electron microscope (SEM).

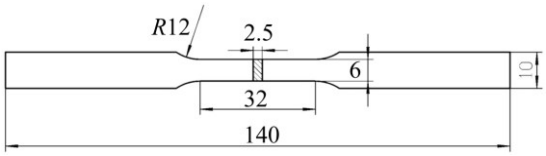

Fig. 3 Dimensions of tensile specimens (Unit: mm)

3 Results and discussion

3.1 Microstructure evolution

By changing the welding speed and laser power, the welding parameters in TC4 and TA15 alloys were researched previously. When the welding speed (v) was too low and laser power (P) was too high, like v= 1 m/min and P=4.1 kW, the heat input was so high that too much metal was molten, as a result, the joint was composed of periodic welding beading and subsidence as shown in Fig. 4(a). When welding speed was as high as 6 m/min and laser power was as low as 2.5 kW, a high quality of continuous weld was unable to form, which resulted from the less production of molten metal just like Fig. 4(b). When the welding speed was controlled from 2 to 5 m/min and the laser power was controlled from 2.5 to 4.1 kW, a good quality of joint could be achieved.

Figures 5 and 6 show the overall cross-sectional macrostructures of the LBWed TC4/TA15 joints under different laser powers and welding speeds, respectively. Fusion zone (FZ) is composed of coarse columnar grains. When laser power increases, the fusion line moves outward from the center, the width of joint expands and the grain size increases. The reason should lie in the heat

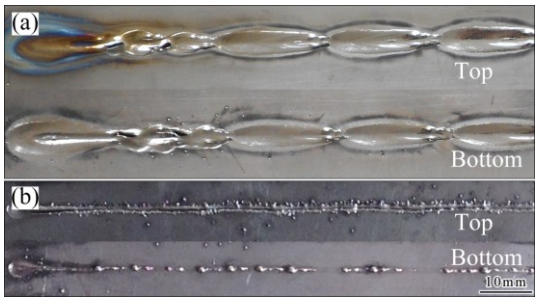

Fig. 4 Macro-morphology of TC4/TA15 LBWed joints under different conditions: (a) v=1 m/min, P=4.1 kW; (b) v=6 m/min, P=2.5 kW

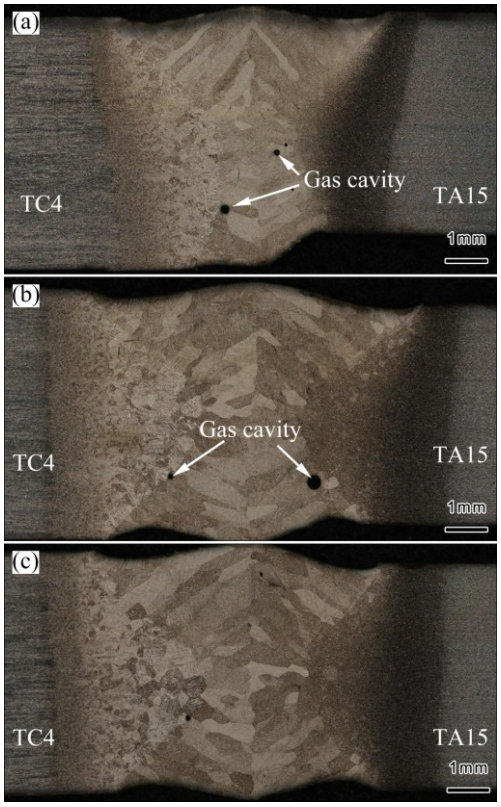

Fig. 5 Cross-sectional macrostructures of TC4/TA15 LBWed joints under different laser powers: (a) 2.5 kW; (b) 3.3 kW; (c) 4.1 kW

input of laser. The higher the laser power is, the larger the heat input is. The area of high temperature becomes larger and the dwell of high temperature increases. The grain of FZ grew in a reverse direction of heat flow and became coarser (Fig. 5). The macro-morphology and outline of the cross-section of joint are mutative with increasing welding speed. For the lower welding speed (2 m/min), weld line energy is higher and there is enough time to make heat uniform. Therefore, the width of joint is almost equivalent along the thickness direction. For the higher welding speed (5 m/min), the joint is narrow due to the lower weld energy input, and the outline of the cross section of joint presents inverted S distribution

(Fig. 6). This is because when keyhole formed by laser beam just passes through workpiece, metal vapor located at the bottom of keyhole blows out downward and prompts molten metal with vast quantities of heat to flow out from bottom of keyhole. As a result, the outline of the cross section of joint is inverted S distribution.

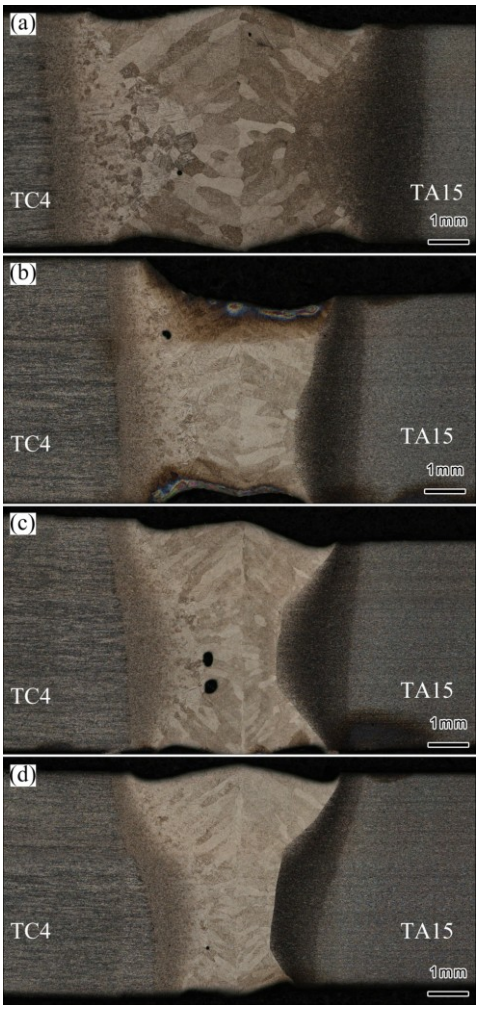

Fig. 6 Cross-sectional macrostructures of TC4/TA15 LBWed joints under different weld speeds: (a) 2 m/min; (b) 3 m/min; (c) 4 m/min; (d) 5 m/min

It can be seen from Figs. 5 and 6 that a certain number of circular gas cavities around boundary of HAZ and FZ can be found. The profile of these gas cavities is almost circular, which are most probably hydrogen cavities [14,15]. At higher temperature, hydrogen integrates into welding bath. The hydrogen cavities will form in the weld when there is no time for the supersaturation of hydrogen to escape from the welding bath during the cooling crystallization process. Solubility of hydrogen in high-temperature titanium decreases with increasing liquid temperature, but it presents saltation at solidification temperature. Temperature in the middle position of the welding bath is higher than that at edge during welding process. The hydrogen in the middle of welding bath diffuses into the center of hydrogen cavities and the boundary of HAZ and FZ. So, hydrogen cavities are formed around the boundary of HAZ and FZ.

Generally, the microstructure of the welded joint mostly depends on the initial microstructure of BM and the thermal cycle, including the heating rate, maximum heating temperature, dwelling time at high temperature and cooling rate [16] during welding process. Figure 7(e) shows the microstructure of FZ. When the joint was cooled rapidly from high temperature, β phase could not transform into α phase just through diffusion and the grain boundary of β phase is reserved. Many scholars [4,10,17] have proved that β phase is forced by shear force to transform into acicular martensite basket-weave microstructure when laser beam is used to weld titanium alloy. Further, the phase transition resistance of β phase increases with the increase of β stabilizer element. Therefore, a higher degree of supercooling was required for the phase transformation, and the martensite start temperature (M_s) was reduced. For this reason, part of the β phases transformed into the slender acicular α phase [10]. Figure 8 gives the result of XRD of FZ, and it proves the existence of α phase. However, both martensite α' and acicular α exhibit a hexagonal structure and their lattice constants are similar, so, XRD could not be used to distinguish them. Generally, Mo equivalents are usually used to evaluate the effect of β stable element on microstructure, and several scholars [18,19] researched the influence of Mo on the phase composition of titanium and found the existence of martensite α' when $[Mo]_{eq}$ is greater than some values. According to the computational formula [20]:

$$[Mo]_{eq}=[Mo]+0.2[Ta]+0.28[Nb]+0.4[W]+0.67[V]+1.25[Cr]+1.25[Ni]+1.7[Mn]+1.7[Co]+2.5[Fe] \quad (1)$$

the Mo equivalents of TC4 and TA15 are 3 and 3.6, respectively, and that of the joint could be regarded as 3.3, which is the average of the two materials. MA et al [3] found martensite α' phase in the FZ and HAZ of laser welded homogeneous TC4 titanium. Therefore, martensite α' is very likely existent in FZ and HAZ.

Figure 7 shows microstructural characteristic of HAZ, and the distribution of microstructure in HAZ is uneven. According to the feature of microstructure, the HAZ of TC4 side can be divided into two zones as shown in Figs. 7(b) and (d). Zone *C* is sited around FZ, the maximum temperature of heating is higher than transition temperature of β phase. So, its microstructure consists of slender acicular α phase and martensite α' phase like FZ. Zone *A* is sited far from FZ, the maximum temperature of heating is lower than transition temperature of β phase. Thus, the microstructure of zone *A* is $\alpha+\beta$ phase. There is no transition of α phase when temperature is higher than martensite start temperature

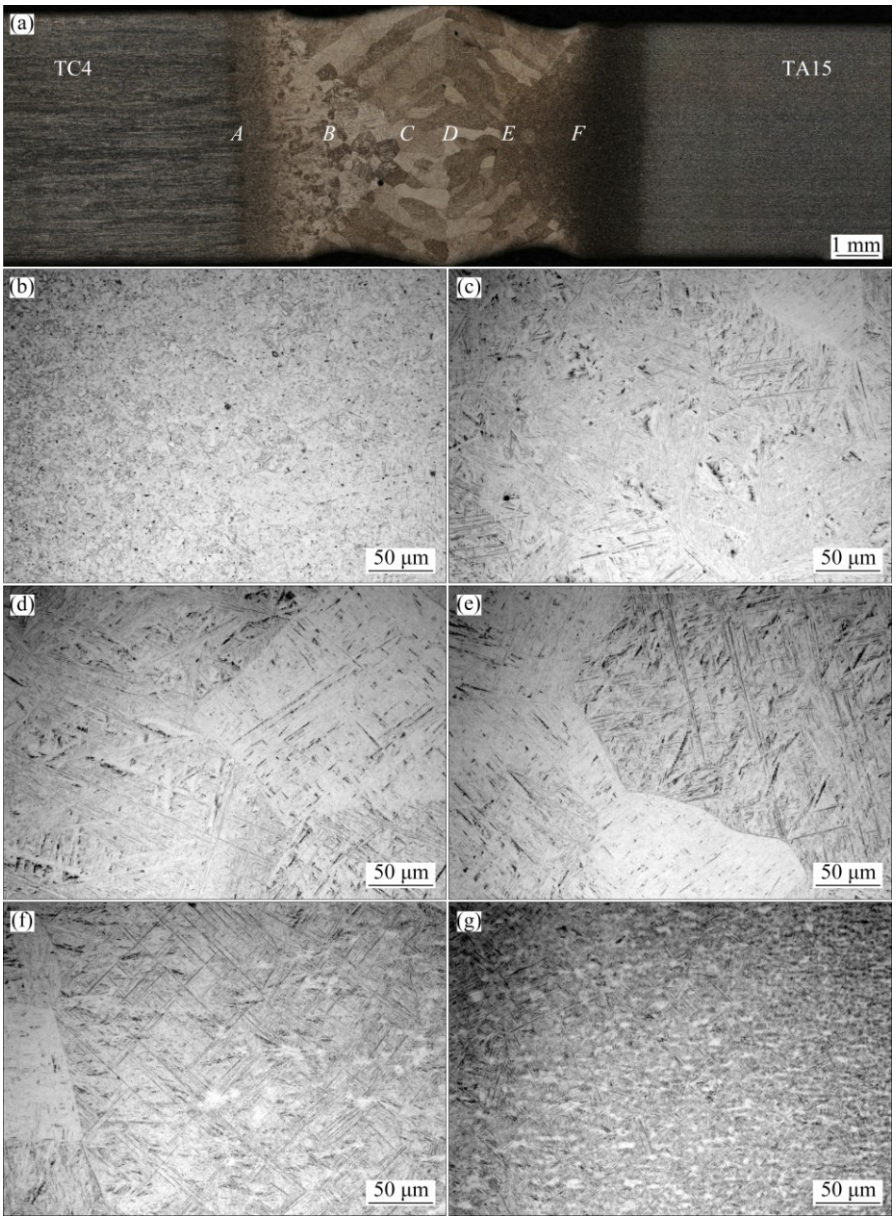

Fig. 7 Microstructures of TC4/TA15 dissimilar LBWed joint: (a) Microstructure including different zones; (b) Zone *A*, outer-HAZ; (c) Zone *B*, middle-HAZ; (d) Zone *C*, inner-HAZ of TC4 side; (e) Zone *D*, centre of the FZ; (f) Zone *E*, inner-HAZ; (g) Zone *F*, outer-HAZ of TA15 side

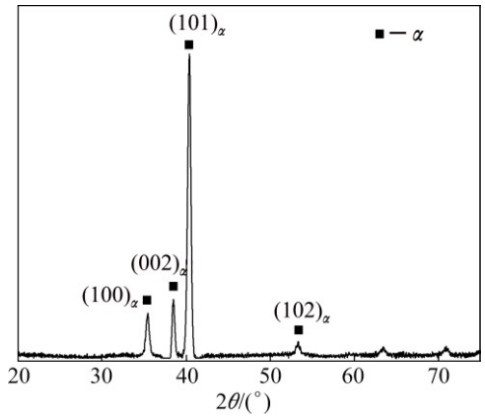

Fig. 8 XRD pattern of fusion zone of dissimilar joint

during the cooling process. Meanwhile, acicular martensite resulted from the lamellar α+β phase and a little equiaxed α phase is precipitated around grain boundary of β phase. The number and size of acicular martensite decrease along with increasing distance far from FZ. Meantime, according to Ref. [17], acicular martensite in TC4 high-energy beam welded joint is parallel.

Similarly, HAZ of TA15 titanium alloy side can be divided into two zones as shown Figs. 7(f) and (g). Unlike HAZ of TC4 side, zone *E* which is near FZ contains quiet a deal equiaxed α phase because the transition temperature of β phase of TA15 is higher than

that of TC4. Therefore, equiaxed α phase is more difficult to transform into acicular martensite in TA15. Moreover, equiaxed α phase grows because of the effect of heat during the cooling process. So, the size of equiaxed α phase in zone *E* is larger than that in zone *F*.

3.2 Microhardness

Figures 9 and 10 show 2D microhardness maps across BM and weld regions of joints. The right-half and the left-half in Figs. 9(a) and 10(a) are microhardness distribution maps of TC4 BM and TA15 BM, respectively. Microhardness value of TA15 BM (about HV 300) is lower than that of TC4 BM (about HV 325), which consists of finer laminar structure. It is easy to find from Figs. 9 and 10 that the microhardness distribution of cross-section of dissimilar joints is asymmetric. According to Ref. [21], the microhardness of phases in welded titanium joint satisfies the order: martensite >α phase >β phase. The maximum values of microhardness were found in the FZ, which was attributed to the massive martensite shown in Fig. 7(e). Although the microhardness value decreased in the HAZ, it was greater than that of the BM due to the formation of intragranular acicular martensite, which became thinner and shorter with increasing the distance away from FZ, as shown in Figs. 7(c) and (d). In HAZ, the microhardness decreased gradually, and the gradient of the two sides is different because of different distributions of microstructure. However, the minimum value of microhardness in the joint was almost the same as the microhardness of BM, which can be used to explain why the tensile samples cracked at the TA15 BM. Similarly, the distribution rule of microhardness was also observed by PANG et al [22].

With the change of welding parameters, the distribution of microhardness is also changed. When laser power increases from 2.5 to 4.1 kW, the width of joint becomes larger, but the maximum value of microhardness is lower and the zone with microhardness value greater than HV 390 is also increased. When

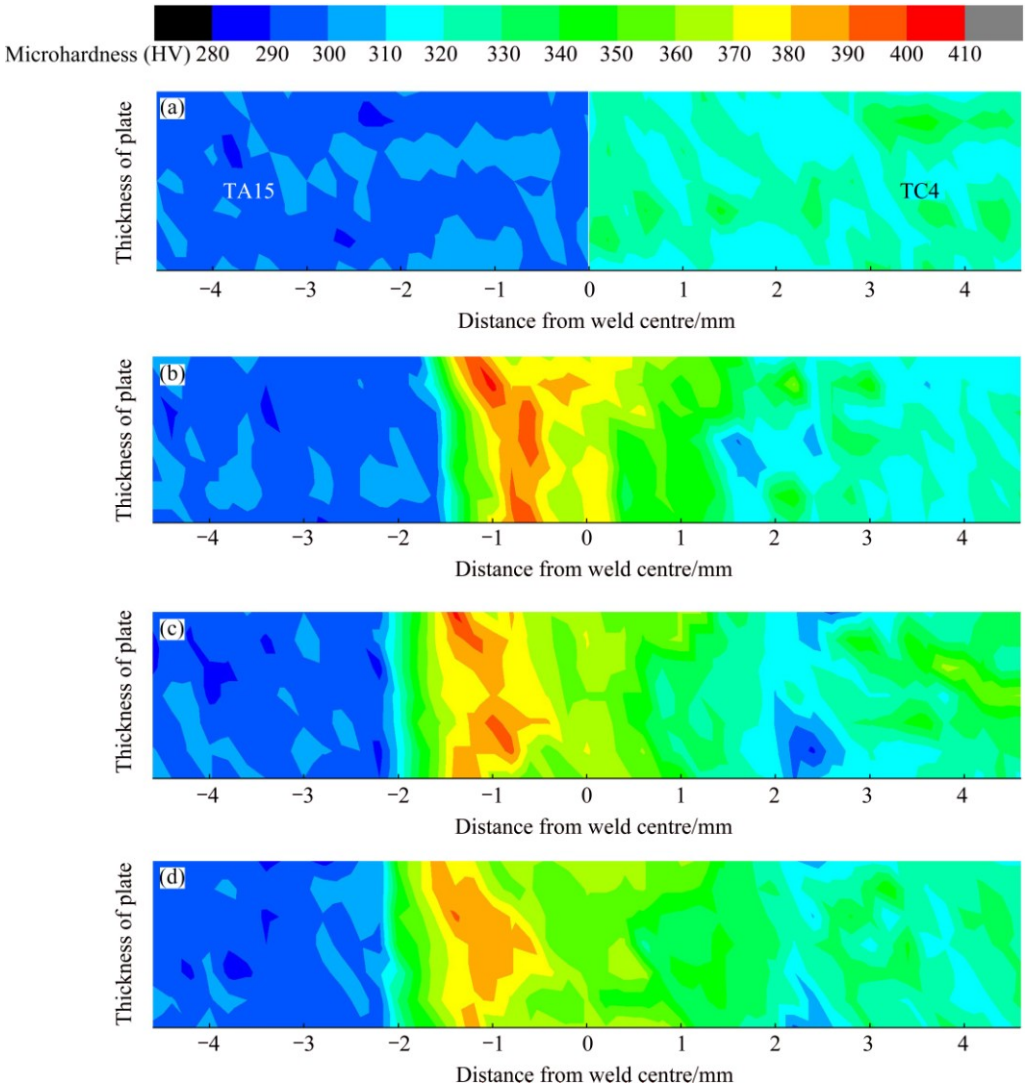

Fig. 9 Microhardness maps of TC4/TA15 LBWed joints under different laser powers: (a) Base material; (b) 2.5 kW; (c) 3.3 kW; (d) 4.1 kW

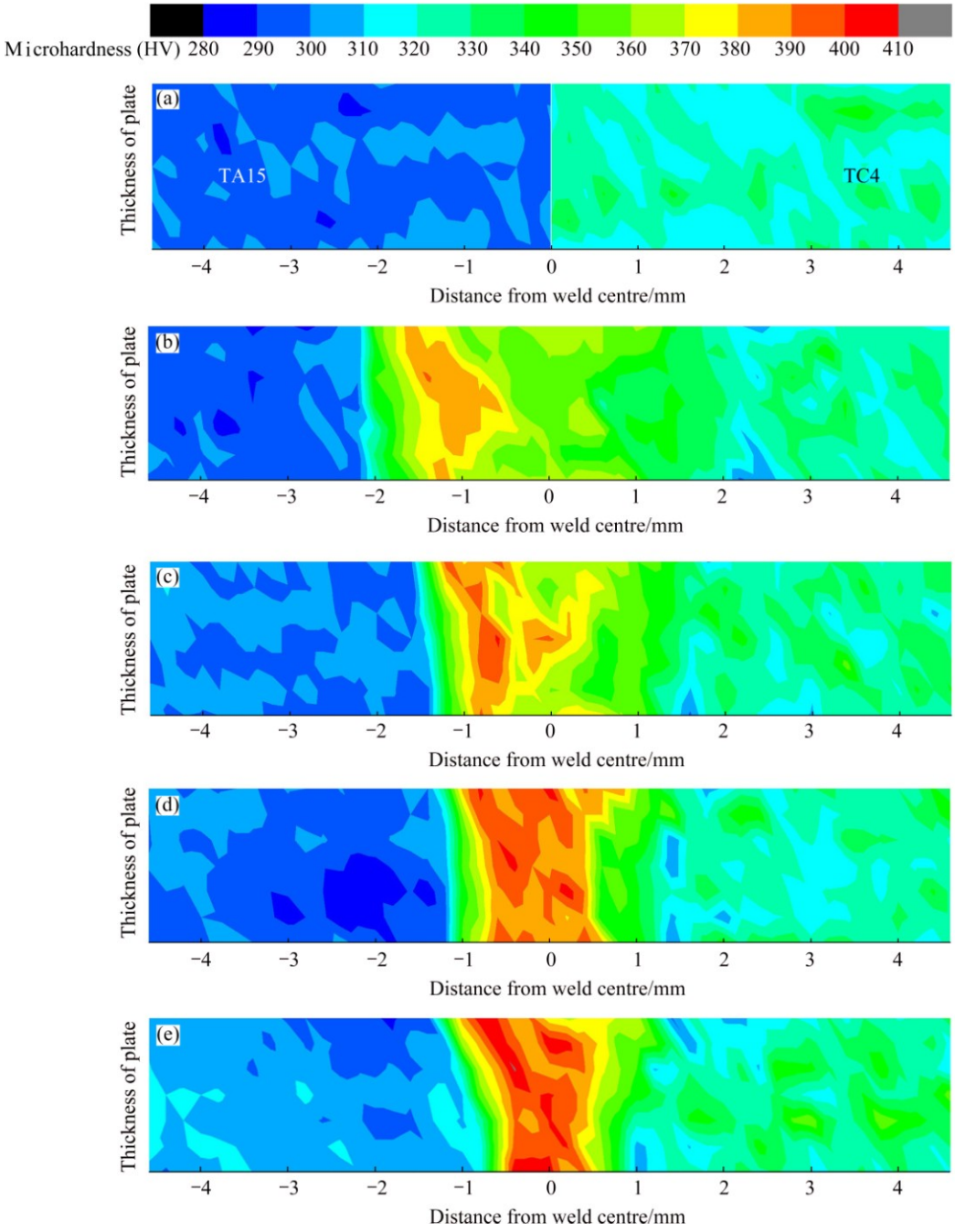

Fig. 10 Microhardness maps of TC4/TA15 LBWed joints under different weld speeds: (a) Base material; (b) 2 m/min; (c) 3 m/min; (d) 4 m/min; (e) 5 m/min

welding speed increases from 2 to 5 m/min, microhardness distribution map also possesses similar phenomenon. When heat input decreases, the cooling rate of joint becomes faster and the effect of quench becomes stronger.

3.3 Tensile properties and strain hardening behavior

Figure 11 gives the changes of tensile properties of BM, similar and dissimilar LBW joints of TC4 and TA15 at different strain rates. The strength and toughness are evaluated by yield strength (YS), ultimate tensile strength (UTS) and static toughness, which can be calculated from the stress vs strain curves of the samples using the Matlab software according to Refs. [23,24]. The strength and toughness of different kinds of joints exhibit considerable variation because they are relevant to the properties of BM. Compared with TA15 titanium alloy, the higher YS and UTS of TC4 titanium alloy are related to its microstructure with a large number of fine plate structures [25,26] and a few interstitial elements like H, N and O (Table 1) provide a stronger resistance for the motion of dislocations during deformation. What

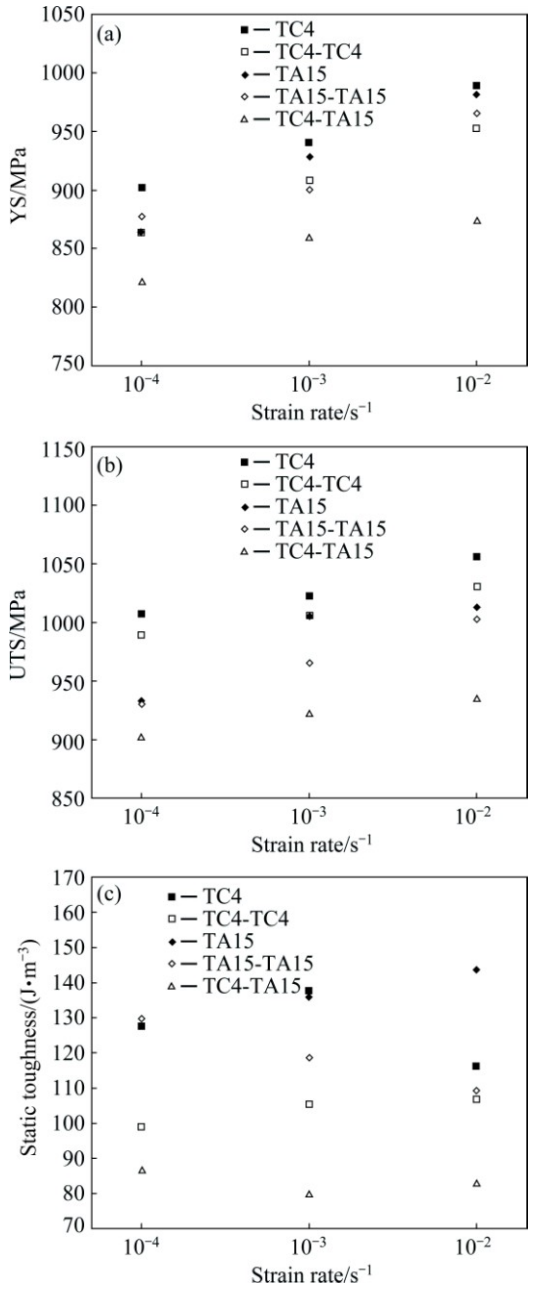

Fig. 11 Tensile properties of titanium dissimilar and similar LBWed joints: (a) YS; (b) UTS; (c) Static toughness

is more, the thermal cycles generated in the laser beam welding process had a significant effect on the tensile behavior of joints. From Fig. 11, TC4 and TA15 titanium alloys showed significantly higher values of YS, UTS and static toughness compared with dissimilar joints of TC4/TA15. For example, at a strain rate of 1×10^{-2} s^{-1}, the YS, UTS and static toughness to failure of TA15 titanium alloy were 982 MPa, 1013 MPa and 143.78 J/m^3, respectively, which were 108 MPa, 78 MPa and 60.98 J/m^3 higher than those of the LBWed dissimilar joints (874 MPa, 935 MPa and 82.80 J/m^3, respectively). The order of tensile strength is as follows: TC4 BM > TC4/TC4 similar joint > TA15 BM > TA15/TA15 similar joint > TC4/TA15 dissimilar joint. It is very interesting to observe that the experiment workpieces led to a pronounced increase in the YS and UTS with increasing strain rate from 1×10^{-4} to 1×10^{-2} s^{-1}. This demonstrates that strain rate has a considerable effect on YS and UTS. For instance, the YS and UTS of TC4/TA15 dissimilar joint increase by 52 MPa and 33 MPa respectively when strain rate increases from 1×10^{-4} to 1×10^{-2} s^{-1}. According to the research of ZHOU and CHEW [27], that is associated with the change of mechanism of plastic flow. In particular, with increasing strain rate, the plastic flow mechanism changed from slippage of dislocation to twin crystals. Besides, SONG et al [28], JAWORSKI and ANKEM [29] also proved that it is reasonable to explain the phenomenon of increasing strength of titanium alloy with increasing strain rate.

Figure 12 shows the effect of welding parameters (laser power and welding speed) on YS and UTS of LBW dissimilar joints in the strain rate range from 1×10^{-4} to 1×10^{-2} s^{-1}. Welding parameters affected the tensile properties of joints significantly. It can be found from Fig. 12 that the TA15 and TC4 titanium alloys had average YS values of 925 and 944 MPa, respectively. The dissimilar joint at a laser power of 4.1 kW had the maximum YS (about 893 MPa) and maximum UTS (about 951 MPa), which were respectively 36 MPa and 29 MPa higher than those of the joint at a laser power of 2.5 kW from Figs. 12(a) and (b). Similarly, from Figs. 12(c) and (d), the YS and UTS of dissimilar joint at a welding speed of 5 m/min were close to those of TA15 titanium alloy. The joint at welding speeds 4 and 3 m/min had an obviously lower YS (with maximum value of 849 MPa) and a lower UTS (with maximum value of 909 MPa) than the TA15 titanium alloy. In particular, among the welding parameters which have been chosen, the joint at 4.1 kW and 5 m/min had the best tensile properties. The YS and UTS increase as strain rate increases from 1×10^{-4} to 1×10^{-2} s^{-1} for all the dissimilar joints. Tensile properties of the joint are associated with its microstructure, which will be affected by thermal cycle [17]. High laser power means high density of energy, and high welding speed means low heat input. When heating rate, dwelling time at high temperature and cooling rate decrease, the maximum microhardness (Figs. 9 and 10) and the strength of the joint are improved.

The hardening capacity was defined as [30],

$$H_c=\frac{\sigma_{UTS}-\sigma_{YS}}{\sigma_{YS}}=\frac{\sigma_{UTS}}{\sigma_{YS}}-1 \quad (2)$$

where σ_{UTS} is UTS and σ_{YS} is YS of the material. Following Eq. (2), the obtained hardening capacity of the laser joints at different welding speeds and laser powers is shown in Fig. 13. Besides, the effect of the strain rate

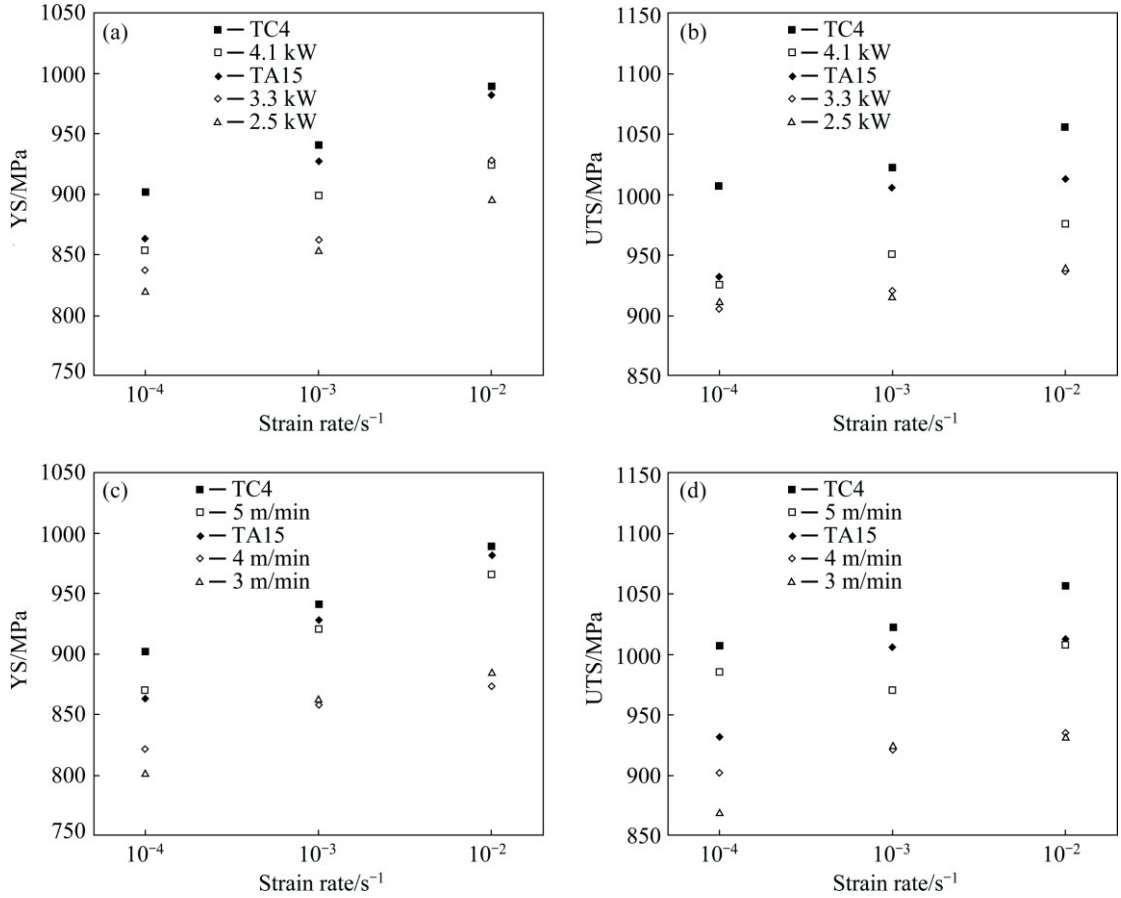

Fig. 12 Effect of strain rate on tensile properties of LBWed joints under different welding parameters of laser powers and welding speeds: (a, b) YS and UTS at welding speed of 2 m/min and varying laser powers, respectively; (c, d) YS and UTS at laser power of 4.1 kW and varying welding speeds, respectively

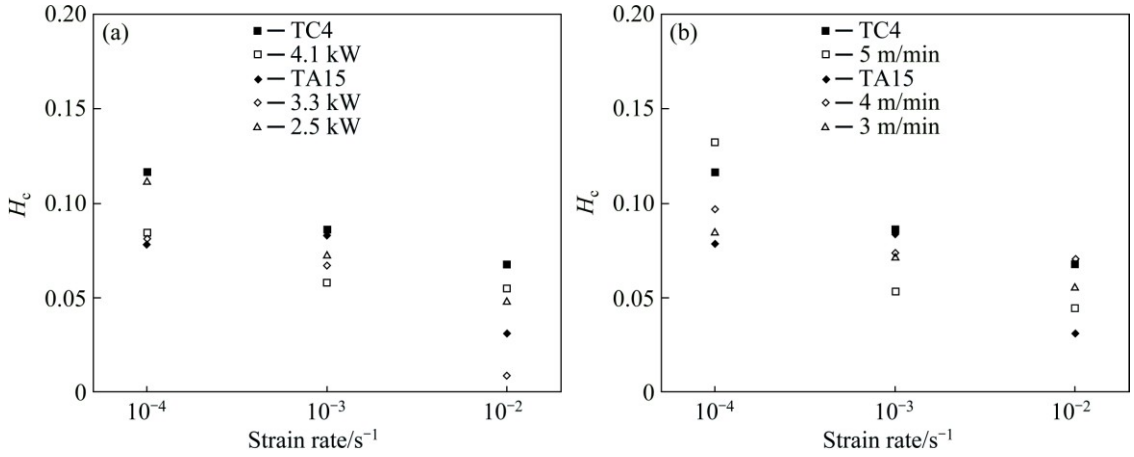

Fig. 13 Effect of strain rate on hardening capacity of dissimilar LBWed joints: (a) H_c values at constant welding speed and varying laser powers; (b) H_c values at constant laser power and varying welding speeds

on hardening capacity is also shown in Fig. 13.

From Fig. 12, the slope of the YS is slightly steeper than that of the UTS with increasing strain rate. Based on Eq. (2), the hardening capacity H_c is related to a YS of material. Generally, when a material was strengthened, the YS increased while the hardening capacity reduced because the capacity of dislocation storage decreased during plastic deformation [30]. With increasing strain rate, the yield stress increased while the hardening capacity decreased. For example, the YS increased by an average of 79.2 MPa and H_c decreased by an average of 0.0548 when laser power changed from 2.5 to 4.1 kW and welding speed was constant. The YS increased by an average of 79.7 MPa and the corresponding value of H_c

decreased by an average of 0.052 when welding speed changed from 3 to 5 m/min and laser power was constant. Therefore, the welding parameters of laser power and welding speed almost have the same effect on the hardening capacity.

To better understand the strain hardening behavior of a material, it is necessary to examine the strain hardening exponent, which represents the ability of a metal to strain hardening, under different strain rates. The larger the strain hardening exponent is, the greater the strain hardening for a given amount of plastic strain is [31,32].

Generally, the strain hardening exponent was defined as

$$\sigma=\sigma_y+K_1\varepsilon^n \quad (3)$$

where σ is true stress and σ_y is yield stress of the material, K_1 is coefficient of microhardness which, in other words, is increment of stress when ε is equal to 1, and n is strain hardening exponent. Figure 14 shows the effect of strain rate on strain hardening exponent of laser joint which was obtained under different welding parameters. With increasing strain rate, the strain hardening exponent of the joints and two kinds of base material decreased. Besides, when strain rate increased from 1×10^{-4} to 1×10^{-2} s^{-1}. The n value of the joints obtained under different laser powers decreased by an average of 0.0318 (Fig. 14(a)), while that of the joints obtained under different welding speeds decreased by an average of 0.0277 (Fig. 14(a)). This means that the laser power and welding speed almost have the same effect on strain hardening behavior of the joint at the stage of plastic deformation. VENKATESH et al [33] also found similar phenomenon when the TC4 ELI was tested. Strain hardening behavior of a material depends on the interaction of dislocation strain filed mostly. Normally, strain hardening of material comes from the multi-slip system and the cross slip during plastic deformation. On the process of multi-slip, the jog formed by the interaction of dislocation inhibits the dislocation motion and results in the strain hardening [34].

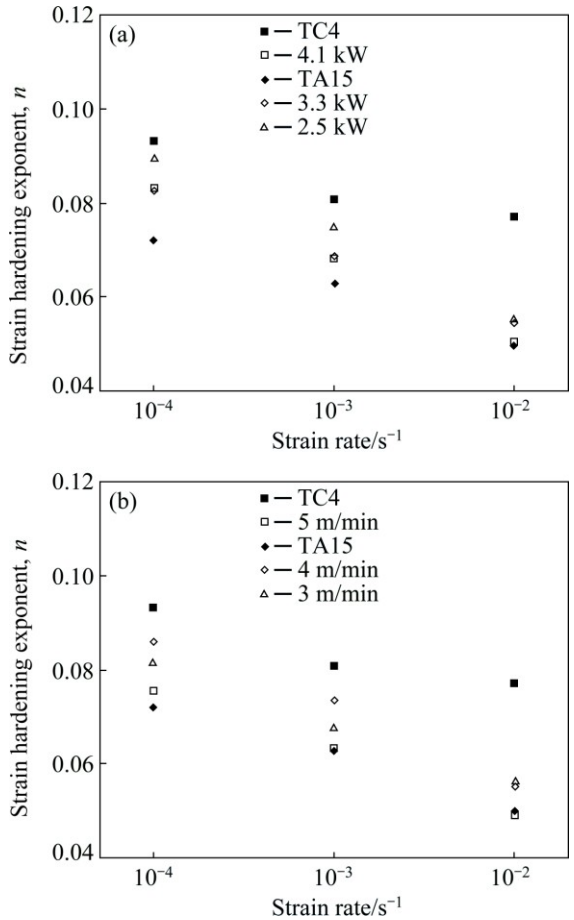

Fig. 14 Effect of strain rate on strain hardening exponent of dissimilar LBWed joints: (a) n values at constant welding speed and varying laser powers; (b) n values at constant laser power and varying welding speeds

3.4 Fracture morphology

The typical macrograph fracture images of tensile samples of the TA15 and TC4 base materials and butt joints at room temperature are shown in Fig. 15. Regardless of the welding parameters, all the tested dissimilar specimens fractured in base material of TA15 alloy which had the lowest microhardness and strength as seen from Figs. 9 and 11 and the fracture position was far from the weld beam. This means that the gas cavity existing in the weld joint did not have an influence on the test property. ZHANG et al [35] demonstrated that there was almost no effect on the bearing capacity of joints within specimens, which exhibited that porosity levels were less than 5.1%. And no specimen failed in FZ, which indicated that the strength of joint was higher than that of TA15 BM. The dull gray and fibrous fracture had a feature of necking and appeared a 45° angle with tensile axis. In general, 45° fracture is attributed to shearing force.

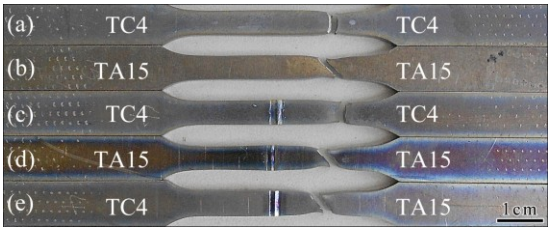

Fig. 15 Typical macrograph fracture images of tensile samples: (a) TC4 BM; (b) TA15 BM; (c) TC4/TC4 joint; (d) TA15/TA15 joint; (e) TC4/TA15 joint

Figure 16 shows the SEM images of TC4/TA15 tensile specimen under different strain rates at room temperature. It can be observed from SEM analysis that

there were equiaxed dimples uniformly distributed on the whole fracture surface. It can be found from Fig. 16 that the density and depth of dimple are larger and larger when strain rate decreases from 1×10^{-2} to 1×10^{-4} s^{-1}, which shows that the toughness of joint is improved. Similar dimple fracture characteristics were also observed in the joints tested by WANG et al [36].

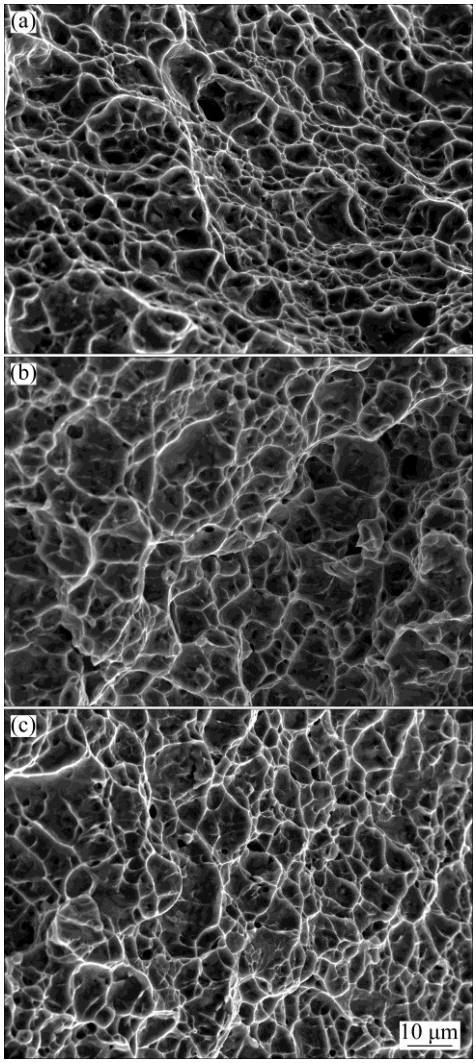

Fig. 16 SEM images showing fracture surfaces of TC4/TA15 LBWed joints tested under different strain rates: (a) 1×10^{-2} s^{-1}; (b) 1×10^{-3} s^{-1}; (c) 1×10^{-4} s^{-1}

4 Conclusions

1) Successful joints are silver white color with homogeneous arc and have no defect. When weld speed is too low, there are welding beadings and caving in the joints. LBWed joints are incomplete penetration when laser power is too low.

2) The fusion zone of TC4/TA15 titanium joint is composed of coarse columnar grains, containing a large number of acicular martensite α phase and slender acicular α phase. HAZ of TA15 side presents equiaxed grains, the size of grain becomes small and the intragranular acicular martensite decreases and becomes thinner and shorter with increasing distance away from FZ. HAZ of TC4 side contains a lot of residual α phases, and a lot of short martensite structures are precipitated around them.

3) The microhardness of the dissimilar joint is significantly higher than that of BM. The width of joint decreases with the decrease of laser power and the increase of welding speed, but the area of high microhardness and maximum value of microhardness increase, which are near TA15 side.

4) The order of tensile strength is as follows: TC4 BM > TC4/TC4 similar joint > TA15 BM > TA15/TA15 similar joint > TC4/TA15 dissimilar joint. Joint connection efficiency is higher than 90%. When strain rate increases, tensile strength of the joint increases while strain hardening capacity and exponent decrease. All the dissimilar joints fail in the BM of TA15 and the fracture is 45° from the tensile axis. Micro-fracture surface of test specimen has characteristics of ductile fracture.

References

[1] YUAN Bao-guo, ZHENG Yu-bin, WANG Yu-jie, GONG Long-qing. Hydrogen absorption characteristics and microstructural evolution of TC21 titanium alloy [J]. Transactions of Nonferrous Metals Society of China, 2016, 26: 599−606.

[2] SINGA S L, YEONGA W Y, WIRIA F E. Selective laser melting of titanium alloy with 50 wt% tantalum: Microstructure and mechanical properties [J]. Journal of Alloys and Compounds, 2016, 660: 461−470.

[3] MA Xu-yi, GONG Shui-li, ZHANG Jiu-xing, LU Wei, YANG Jing. Formation, microstructure and mechanical properties of double-sided laser beam welded Ti−6Al−4V T-joint [J]. Transactions of Nonferrous Metals Society of China, 2016, 26: 729−735.

[4] QI Yun-lian, DENG Ju, HONG Quan, ZENG Li-ying. Electron beam welding, laser beam welding and gas tungsten arc welding of titanium sheet [J]. Materials Science and Engineering A, 2000, 280: 177−181.

[5] SUN Q J, WANG G C. Microstructure and superplasticity of TA15 alloy [J]. Materials Science and Engineering A, 2014, 606: 401−408.

[6] WANG S Q, LIU J H, CHEN D L. Strain-controlled fatigue properties of dissimilar weld joints between Ti−6Al−4V and Ti17 alloys [J]. Materials & Design, 2013, 49: 716−727.

[7] CAM G, KOCAK M, DOS SANTOS J F. Development in laser welding of metallic materials and characterization of the joints [J]. Welding in the World, 1999, 43(2): 13−26.

[8] LEI Z L, DONG Z J, CHEN Y B, HUANG L, ZHU R C. Microstructure and mechanical properties of laser welded Ti−22Al−27Nb/TC4 dissimilar alloys [J]. Materials Science and Engineering A, 2013, 559: 909−916.

[9] QIAN Ting-ting, LIU Dong, TIAN Xiang-jun, LIU Chang-meng, WANG Hua-ming. Microstructure of TA2/TA15 graded structural material by laser additive manufacturing process [J]. Transactions of Nonferrous Metals Society of China, 2014, 24: 2729−2736.

[10] ZHANG Hao, HU Sheng-sun, SHEN Jun-qi, LI Da-long, BU Xian-zheng. Effect of laser beam offset on microstructure and mechanical properties of pulsed laser welded BTi−6431S/TA15 dissimilar titanium alloys [J]. Optics & Laser Technology, 2015, 74: 158−166.

[11] CHEN Shu-hai, LI Li-qun, CHEN Yan-bing, HUANG Ji-hua. Joining

mechanism of Ti/Al dissimilar alloys during laser welding-brazing process [J]. Journal of Alloys and Compounds, 2011, 509: 891−898.
[12] TOMASHCHUK I, SALLAMAND P, CICALA E, GREVEY D. Direct keyhole laser welding of aluminum alloy AA5754 to titanium alloy Ti6Al4V [J]. Journal of Materials Processing Technology, 2015, 217: 96−104.
[13] CHEN Shu-hai, ZHANG Ming-xin, HUANG Ji-hua, CUI Cheng-ji, ZHANG Hua, ZHAO Xing-ke. Microstructures and mechanical property of laser butt welding of titanium alloy to stainless steel [J]. Materials & Design, 2014, 53: 504−511.
[14] ELIEZER D, TAL-GUTELMACHER E, CROSS C E, BOELLINGHAUS T. Hydrogen absorption and desorption in a duplex-annealed Ti−6Al−4V alloy during exposure to different hydrogen-containing environments [J]. Materials Science and Engineering A, 2006, 433: 298−304.
[15] HUANG J L, WARNKEN N, GEBELIN J C, STRANGWOOD M, REED E C. On the mechanism of porosity formation during welding of titanium alloys [J]. Acta Materialia, 2012, 60: 3215−3225.
[16] LU Wei, SHI Yao-wu, LEI Yong-ping, LI Xiao-yan. Effect of electron beam welding on the microstructures and mechanical properties of thick TC4-DT alloy [J]. Materials & Design, 2012, 34: 509−515.
[17] WANG S Q, LIU J H, CHEN D L. Tensile and fatigue properties of electron beam welded dissimilar joints between Ti−6Al−4V and BT9 titanium alloys [J]. Materials Science and Engineering A, 2013, 584: 47−56.
[18] HO W F, JU C P, LIN J H C. Structure and properties of cast binary Ti−Mo alloy [J]. Biomaterials, 1999, 20: 2115−2122.
[19] OLIVEIRA N T C, ALEIXO G, CARAM R, GUASTALDI A C. Development of Ti−Mo alloys for biomedical applications: Microstructure and electrochemical characterization [J]. Materials Science and Engineering A, 2007, 452−453: 727−731.
[20] LÜERING G, WILLIANS J C. Engineering materials and process: titanium [M]. Heideberg: Springer, 2003.
[21] LI Xing-zhi, HU Shu-bing, XIAO Jian-zhong, JI Long-bo. Effects of the heterogeneity in the electron beam welded joint on fatigue crack growth in Ti−6Al−4V alloy [J]. Materials Science and Engineering A, 2011, 529: 170−176.
[22] PANG Qi-hang, ZHAO Zheng-zhi, TANG Di. Microstructure and properties of hot-rolled high strength bainitic steel by laser welding [J]. Materials & Design, 2015, 87: 363−369.
[23] ZHANG Ling-yi, YANG Gang, HUANG Chong-xiang, CHEN Wei-liang, WANG Li-min. High strength and high toughness heat-resistant martensitic steel produced by ECAP [J]. Acta Metallurgica Sinica, 2008, 44: 409−413. (in Chinese)
[24] ZHANG Zhi-min, ZHANG Xing, WANG Qiang, LI Bao-cheng. Research on lightweight design of heavy vehicle transmission and action components [J]. Journal of Mechanical Engineering, 2012, 48: 67−71.
[25] FACCHINI L, MOLINARI A, HÖGES S, WISSENBACH K. Ductility of a Ti−6Al−4V alloy produced by selective laser melting of prealloyed powders [J]. Rapid Prototyping Journal, 2010, 16: 450−459.
[26] NALLA R K, BOYCE B L, CAMPBELL J P, PETRES J O, RITCHIE R O. Influence of microstructure on high-cycle fatigue of Ti−6Al−4V: Bimodal vs. lamellar structures [J]. Metallurgical and Materials Transaction A, 2002, 33: 899−918.
[27] ZHOU W, CHEW K G. The rate dependent response of a titanium alloy subjected to quasi-static loading in ambient environment [J]. Journal of Materials Science, 2002, 37: 5159−5165.
[28] SONG Hong-wu, ZHANG Shi-hong, CHENG Ming. Subtransus deformation mechanisms of TC11 titanium alloy with lamellar structure [J]. Transactions of Nonferrous Metals Society of China, 2010, 20: 2168−2173.
[29] JAWORSKI A, ANKEM S. The effect of α phase on the deformation mechanisms of β titanium alloys [J]. Journal of Materials Engineering and Performance, 2005, 14: 755−760.
[30] AFRIN N, CHEN D L, CAO X, JAHAZI M. Strain hardening behavior of a friction stir welded magnesium alloy [J]. Scripta Materialia, 2007, 57: 1004−1007.
[31] XU W F, LIU J H, CHEN D L, LUAN G H, YAO J S. Improvements of strength and ductility in aluminum alloy joints via rapid cooling during friction stir welding [J]. Materials Science and Engineering A, 2012, 57: 89−98.
[32] LOU S, NORTHWOOD D O. Effect of strain aging on the strength coefficient and strain-hardening exponent of construction-grade steel [J]. Journal of Materials Engineering and Performance, 1994, 3: 344−349.
[33] VENKATESH B D, CHEN D L, BHOLE S D. Effect of heat treatment on mechanical properties of Ti−6Al−4V ELI alloy [J]. Materials Science and Engineering A, 2009, 506: 117−124.
[34] VALLE J A, CARREÑO F, RUANO O A. Influence of texture and grain size on work hardening and ductility in magnesium-based alloys [J]. Acta Materialia, 2006, 54: 4247−4259.
[35] ZHANG Yu-feng, HUO Li-xing, JING Hong-yang, PAN Rui-hong. The effects of porosities and slag inclusions on mechanical properties of welded joint [J]. Pressure Vessel Technology, 1996, 13: 34−38. (in Chinese)
[36] WANG S Q, LIU J H, CHEN D L. Effect of strain rate and temperature on strain hardening behavior of a dissimilar joint between Ti−6Al−4V and Ti17 alloys [J]. Materials & Design, 2014, 56: 174−184.

TC4/TA15 异质钛合金激光焊焊缝的显微组织和力学性能

徐韦锋[1,2]，张振林[1,2]

1. 西北工业大学 凝固技术国家重点实验室，西安 710072；
2. 西北工业大学 陕西省摩擦焊接技术实验室，西安 710072

摘　要：研究 TC4/TA15 异质钛合金激光焊焊缝的显微组织和力学性能。结果表明：TC4/TA15 异质钛合金激光焊缝熔合区显微组织由针状 α 相和马氏体 α'组成，TC4 侧热影响区主要是残余 α 相和马氏体 α'，TA15 侧热影响区则出现了大量等轴 α 相。焊缝显微硬度呈现不对称特征，熔合区最高，TA15 母材区最低。随应变速率由 1×10^{-4} s^{-1} 增加到 1×10^{-2} s^{-1}，接头屈服强度和抗拉强度均升高，且满足 TC4 母材>TC4/TC4 同质接头>TA15 母材>TA15/TA15 同质接头>TC4/TA15 异质接头，而硬化能力和应变硬化指数则降低。不同应变速率下拉伸 TC4/TA15 异质接头均在 TA15 母材断裂，断口呈现韧性断裂特征。

关键词：激光焊；钛合金；异质接头；变应速率；显微组织；力学性能

(Edited by Wei-ping CHEN)